

# DaDianNao: A Machine-Learning Supercomputer

Yunji Chen<sup>1</sup>, Tao Luo<sup>1,3</sup>, Shaoli Liu<sup>1</sup>, Shijin Zhang<sup>1</sup>, Liqiang He<sup>2,4</sup>, Jia Wang<sup>1</sup>, Ling Li<sup>1</sup>,  
Tianshi Chen<sup>1</sup>, Zhiwei Xu<sup>1</sup>, Ninghui Sun<sup>1</sup>, Olivier Temam<sup>2</sup>

<sup>1</sup> SKL of Computer Architecture, ICT, CAS, China

<sup>2</sup> Inria, Scalay, France

<sup>3</sup> University of CAS, China

<sup>4</sup> Inner Mongolia University, China

**Abstract**—Many companies are deploying services, either for consumers or industry, which are largely based on machine-learning algorithms for sophisticated processing of large amounts of data. The state-of-the-art and most popular such machine-learning algorithms are Convolutional and Deep Neural Networks (CNNs and DNNs), which are known to be both computationally and memory intensive. A number of neural network accelerators have been recently proposed which can offer high computational capacity/area ratio, but which remain hampered by memory accesses.

However, unlike the memory wall faced by processors on general-purpose workloads, the CNNs and DNNs memory footprint, while large, is not beyond the capability of the on-chip storage of a multi-chip system. This property, combined with the CNN/DNN algorithmic characteristics, can lead to high internal bandwidth and low external communications, which can in turn enable high-degree parallelism at a reasonable area cost. In this article, we introduce a custom multi-chip machine-learning architecture along those lines. We show that, on a subset of the largest known neural network layers, it is possible to achieve a speedup of 450.65x over a GPU, and reduce the energy by 150.31x on average for a 64-chip system. We implement the node down to the place and route at 28nm, containing a combination of custom storage and computational units, with industry-grade interconnects.

## I. INTRODUCTION

Machine-Learning algorithms have become ubiquitous in a very broad range of applications and cloud services; examples include speech recognition, e.g., Siri or Google Now, click-through prediction for placing ads [27], face identification in Apple iPhoto or Google Picasa, robotics [20], pharmaceutical research [9] and so on. It is probably not exaggerated to say that machine-learning applications are in the process of displacing scientific computing as the major driver for high-performance computing. Early symptoms of this transformation are Intel calling for a refocus on Recognition, Mining and Synthesis applications in 2005 [14] (which later led to the PARSEC benchmark suite [3]), with Recognition and Mining largely corresponding to machine-learning tasks, or IBM developing the Watson supercomputer, illustrated with the Jeopardy game in 2011 [19].

Remarkably enough, at the same time this profound shift in applications is occurring, two simultaneous, albeit apparently unrelated, transformations are occurring in the machine-learning and in the hardware domains. Our community is well aware of the trend towards heterogeneous computing where architecture specialization is seen as a promising path to achieve high performance at low energy [21], provided we can find ways to reconcile architecture specialization and flexibility. At the same time, the machine-learning domain has profoundly evolved since 2006, where a category of algorithms, called Deep Learning (Convolutional and Deep Neural Networks), has emerged as state-of-the-art across a broad range of applications [33], [28], [32], [34]. In other words, at the time where architects need to find a good tradeoff between flexibility and efficiency, it turns out that just one category of algorithms can be used to implement a broad range of applications. In other words, there is a fairly unique opportunity to design highly specialized, and thus highly efficient, hardware which will benefit many of these emerging high-performance applications.

A few research groups have started to take advantage of this special context to design accelerators meant to be integrated into heterogeneous multi-cores. Temam [47] proposed a neural network accelerator for multi-layer perceptrons, though it is not a deep learning neural network, Esmaeilzadeh et al. [16] propose to use a hardware neural network called NPU for approximating any program function, though not specifically for machine-learning applications, Chen et al. [5] proposed an accelerator for Deep Learning (CNNs and DNNs). However, all these accelerators have significant neural network *size* limitations: either small neural networks of a few tens of neurons can be executed, or the neurons and synapses (i.e., weights of connections between neurons) intermediate values have to be stored in main memory. These two limitations are severe, respectively from a machine-learning or a hardware perspective.

From a machine-learning perspective, there is a significant trend towards increasingly large neural networks. The recent work of Krizhevsky et al. [32] achieved state-of-the-art accuracy on the ImageNet database [13] with “only” 60

million parameters. There are recent examples of a 1-billion parameter neural network [34], and some of the same authors even investigated a 10-billion neural network the following year [8]. However, these networks are for now considered extreme experiments in unsupervised learning (the first one on 16,000 CPUs, the second one on 64 GPUs), and they are outperformed by smaller but more classic neural networks such as the one by Krizhevsky et al. [32]. Still, while the neural network size progression is unlikely to be monotonic, there is a definite trend towards larger neural networks. Moreover, increasingly large inputs (e.g., HD instead of SD images) will further inflate the neural networks sizes. From a hardware perspective, the aforementioned accelerators are limited because if most synaptic weights have to reside in main memory, and if neurons intermediate values have to be frequently written back and read from memory, the memory accesses become the performance bottleneck, just like in processors, partly voiding the benefit of using custom architectures. Chen et al. [5] acknowledge this issue by observing that their neural network accelerator loses at least an order of magnitude in performance due to memory accesses.

However, while 1 billion parameters or more may come across as a large number from a machine-learning perspective, it is important to realize that, in fact, it is not from a hardware perspective: if each parameter requires 64 bits, that only corresponds to 8 GB (and there are clear indications that fewer bits are sufficient). While 8 GB is still too large for a single chip, it is possible to imagine a dedicated machine-learning computer composed of multiple chips, each chip containing specialized logic together with enough RAM that the sum of the RAM of all chips can contain the *whole* neural network, requiring *no main memory*. By tightly interconnecting these different chips through a dedicated mesh, one could implement the largest existing DNNs, achieve high performance at a fraction of the energy and area of the many CPUs or GPUs used so far. Due to its low energy and area costs, such a machine, a kind of compact machine-learning supercomputer, could help spread the use of high-accuracy machine-learning applications, or conversely to use even larger DNNs/CNNs by simply scaling up RAM storage at each node and/or the number of nodes.

In this article, we present such an architecture, composed of interconnected nodes, each containing computational logic, eDRAM, and the router fabric; the node is implemented down to the place and route at 28nm, and we evaluate an architecture with up to 64 nodes. On a sample of the largest existing neural network layers, we show that it is possible to achieve a speedup of 450.65x over a GPU and to reduce energy by 150.31x on average.

In Section II, we introduce CNNs and DNNs, in Section III, we evaluate such NNs on GPU, in Section IV we compare GPU and a recently proposed accelerator for CNNs and DNNs, in Section V, we introduce the machine-learning

supercomputer, we present the methodology in Section VI, the experimental results in Section VII and the related work in Section VIII.

## II. STATE-OF-THE-ART MACHINE-LEARNING TECHNIQUES

The state-of-the-art and most popular machine-learning algorithms are Convolutional Neural Networks (CNNs) [35] and Deep Neural Networks (DNNs) [9]. Beyond early differences in training, the two types of networks are also distinguished by their implementation of convolutional layers detailed thereafter. CNNs are particularly efficient for image applications and any application which can benefit from the implicit translation invariance properties of their convolutional layers. DNNs are more complex neural networks but they have an even broader application span such as speech recognition [9], web search [27], etc.

### A. Main Layer Types

A CNN or a DNN is a sequence of multiple instances of four types of layers: pooling layers (POOL), convolutional layers (CONV), classifier layers (CLASS), and local response normalization layers (LRN), see Figure 1. Usually, groups of convolutional, local response normalization and pooling layers alternate, while classifier layers are found at the end of the sequence, i.e., at the top of the neural network hierarchy. We present a simple hierarchy in Figure 1; we illustrate the intuitive task performed at the top, and we provide the formal computations performed by the layer at the bottom.

*Convolutional layers (CONV).* Intuitively, a convolutional layer implements a set of filters to identify characteristic elements of the input data, e.g., an image, see Figure 1. For visual data, a filter is defined by  $K_x \times K_y$  coefficients forming a *kernel*; these kernel coefficients are learned and form the layer synaptic weights. Each convolutional layer slides  $N_{of}$  such filters through the whole input layer (by steps of  $s_x$  and  $s_y$ ), resulting in as many ( $N_{of}$ ) output feature maps.

The concrete formula for calculating an output neuron  $a(x, y)^{f_o}$  at position  $(x, y)$  of output feature map  $f_o$  is

$$out(x, y)^{f_o} = \sum_{i=0}^{N_{if}} \sum_{k_x=0}^{K_x} \sum_{k_y=0}^{K_y} w_{f_i, f_o}(k_x, k_y) * in(x + k_x, y + k_y)^{f_i}$$

where  $in(x, y)^f$  (resp.  $out()$ ) represents the input (resp. output) neuron activity at position  $(x, y)$  in feature map  $f$ , and  $w_{f_i, f_o}(k_x, k_y)$  is the synaptic weight at kernel position  $(k_x, k_y)$  in input feature map  $f_i$  for filter (output feature map)  $f_o$ . Since the input layer itself may contain multiple feature maps ( $N_{if}$  input feature maps), the kernel is usually three-dimensional, i.e.,  $K_x \times K_y \times N_{if}$ .

In DNNs, the kernels usually have different synaptic values for each output neuron (at each  $(x, y)$  position), while

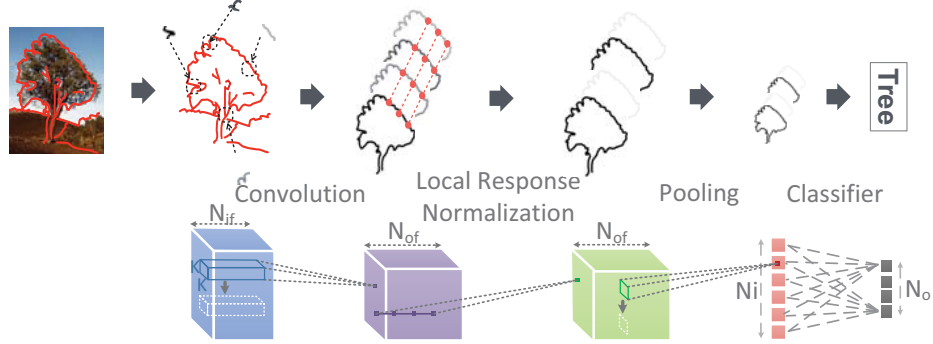


Figure 1: The four layer types found in CNNs and DNNs.

in CNNs, the kernels are *shared* across all neurons of the same output feature map. Convolutional layers with private (non-shared) kernels have *drastically more* synaptic weights (i.e., parameters) than the ones with shared kernels ( $K \times K \times N_{if} \times N_{of} \times N_x \times N_y$  vs.  $K \times K \times N_{if} \times N_{of}$ , where  $N_x$  and  $N_y$  are the input layer dimensions).

*Pooling layers (POOL).* A pooling layer computes the max or average over a number of neighbor points, e.g.,

$$out(x, y)^f = \max_{0 \leq k_x \leq K_x, 0 \leq k_y \leq K_y} in(x + k_x, y + k_y)^f$$

Its effect is to reduce the input layer dimensionality, which allows coarse-grain (larger scale) features to emerge, see Figure 1, and be later identified by filters in the next convolutional layers. Unlike a convolutional or a classifier layer, a pooling layer has no learned parameter (no synaptic weight).

*Local response normalization layers (LRN).* Local response normalization implements competition between neurons at the same location, but in different (neighbor) feature maps. Krizhevsky et al. [32] postulate that their effect is similar to the lateral inhibition found in biological neurons. The computations are as follows

$$out(x, y)^f = in(x, y)^f / \left( c + \alpha \sum_{g=\max(0, f-k/2)}^{\min(N_f-1, f+k/2)} (a(x, y)^g)^2 \right)^\beta$$

where  $k$  determines the number of adjacent feature maps considered, and  $c$ ,  $\alpha$  and  $\beta$  are constants.

*Classifier layers (CLASS).* The result of the sequence of CONV, POOL and LRN layers is then fed to one or multiple classifier layers. This layer is typically fully connected to its  $N_i$  inputs (and it has  $N_o$  outputs), see Figure 1, and each connection carries a learned synaptic weight. While the number of inputs may be much lower than for other layers (due to the dimensionality reduction of pooling layers), they can account for a large share of all synaptic weights in the neural network due to their full connectivity. Multi-Layer

perceptrons are frequently used as classifier layers, though other types of classifiers are used as well (e.g., multinomial logistic regression). The goal of these layers is naturally to correlate the different features extracted from the filtering, normalization and pooling steps and the output categories.

$$out(j) = t \left( \sum_{i=0}^{N_i} w_{ij} * in(i) \right)$$

where  $t()$  is a transfer function, e.g.,  $\frac{1}{1+e^{-x}}$ ,  $\tanh(x)$ ,  $\max(0, x)$  for ReLU [32], etc.

## B. Benchmarks

Throughout this article, we use as benchmarks a sample of 10 of the largest known layers of each type, described in Table I, as well as a full neural network (CNN), winner of the ImageNet 2012 competition [32]. The full NN benchmark contains the following 12 layers (the format is  $N_x, N_y, K_x, K_y, N_i$  or  $N_{if}, N_o$  or  $N_{of}$  as in the table): CONV (224,224,11,11,3,96), LRN (55,55,-,-,96,96), POOL (55,55,3,3,96,96), CONV (27,27,5,5,96,256), LRN (27,27,-,-,256,256), POOL (27,27,3,3,256,256), CONV (13,13,3,3,256,384), CONV (13,13,3,3,384,384), CONV (13,13,3,3,384,256), CLASS (-,-,-,-,9216,4096), CLASS (-,-,-,-,4096,4096), CLASS (-,-,-,-,4096,1000). For all convolutional layers, the sliding window strides  $s_x, s_y$  are 1, except for the first convolutional layer of the full NN, where they are 4. For all pooling layers, their sliding window strides equal to their kernel dimension, i.e.  $s_x = K_x$ ,  $s_y = K_y$ . Note also that for LRN layers,  $k = 5$ . Finally, since we consider both inference and training for each layer, see Section II-C, we have also considered the most popular *pre-training* method, i.e., the method used to initialize the synaptic weights, which is often time-consuming. This method is based on Restricted Boltzmann Machines (RBM) [45], and we applied it to CLASS1 and CLASS2 layers, leading to the RBM1 (2560×2560) and RBM2 (4096×4096) benchmarks.

## C. Inference vs. Training

A frequent and important misconception about neural networks is that *on-line* learning (a.k.a. training or backward

Layer	$N_x$	$N_y$	$K_x$	$K_y$	$N_i$	$N_o$	Synapses Description	
	or $N_i$ for $N_o$							
CLASS1	-	-	-	-	2560	2560	12.5MB	Object recognition and speech recognition tasks (DNN) [11].
CLASS2	-	-	-	-	4096	4096	32MB	Multi-Object recognition
CONV1	256	256	11	11	256	384	22.69MB	in natural images (DNN),
POOL2	256	256	2	2	256	256	-	winner 2012 ImageNet
LRN1	55	55	-	-	96	96	-	competition [32].
LRN2	27	27	-	-	256	256	-	
CONV2	500	375	9	9	32	48	0.24MB	Street scene parsing (CNN) (e.g., identifying building, vehicle, etc) [18].
POOL1	492	367	2	2	12	12	-	
CONV3*	200	200	18	18	8	8	1.29GB	Face Detection in YouTube videos (DNN), (Google) [34].
CONV4*	200	200	20	20	3	18	1.32GB	YouTube video object recognition, largest NN to date [8].

Table I: Some of the largest known CNN or DNN layers (CONVx\* indicates convolutional layers with private kernels).

phase) is necessary for many applications. On the contrary, for many industrial applications *off-line* learning is sufficient, where the neural network is first trained on a set of data, and then only used in inference (a.k.a. testing or feed-forward phase) mode by the end user. Note that even machine-learning researchers acknowledge this choice, as one of the few examples of hardware designs coming from that community is dedicated to inference [18]. While we put more emphasis in design and experiments on the much broader market of *users* of machine-learning algorithms, we have also designed the architecture to support the most common learning algorithms in order to also serve as an accelerator for machine-learning *researchers* and we also present experiments for that usage.

### III. THE GPU OPTION

Currently, the most favored approach for implementing CNNs and DNNs are GPUs [6] due to the fairly regular nature of these algorithms. We have implemented in CUDA the different layer types of Table I. We have also implemented a C++ version in order to obtain a CPU (SIMD) baseline. We have evaluated these versions on respectively a modern GPU card (NVIDIA K20M, 5GB GDDR5, 208 GB/s memory bandwidth, 3.52 TFlops peak, 28nm technology), and a 256-bit SIMD CPU (Intel Xeon E5-4620 Sandy Bridge-EP, 2.2GHz, 1TB memory); we report the speedups of GPU over CPU (for inference) in Figure 2. The GPU can provide a speedup of 58.82x over a SIMD on average. This is in line with state-of-the-art results, for instance reported by Ciresan et al. [7], where speedups of 10x for the smallest layers to 60x for the largest layers are reported for an NVIDIA GTX480/GTX580 over an Intel Core-i7 920 on CNNs. One can also observe that the GPU is particularly efficient on LRN layers because of the presence of a dedicated

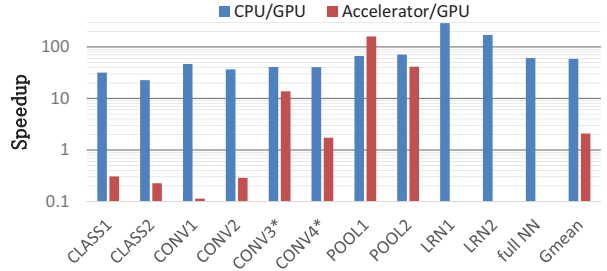


Figure 2: Speedup of GPU over CPU (SIMD) and DianNao accelerator [5].

exponential instruction, a computation which accounts for most the LRN execution time on SIMD.

While these speedups are high, GPUs have a number of limitations. First, their (area) cost is high because of both the number of hardware operators *and* the need to remain reasonably general-purpose (memory hierarchy, all PEs are connected to some elements of the memory hierarchy, etc). Second, the total execution time remains large (up to 18.03 seconds for the largest layer CLASS1); this may not be compatible with the milliseconds response time required by web services or other industrial applications. Third, the GPU energy efficiency is moderate, with an average power of over 74.93W for the NVIDIA K20M GPU. That figure is actually optimistic because the NVIDIA K20M only contains 1.5MB of on-chip RAM, forcing frequent high-energy accesses to the off-chip GDDR5 memory leading to a thermal design power of 225W for the entire GPU board [43].

### IV. THE ACCELERATOR OPTION

Recently, Chen et al. [5] have proposed the DianNao accelerator for the fast and low-energy execution of the inference of large CNNs and DNNs in a small form factor ( $3\text{mm}^2$  at 65nm, 0.98GHz). We reproduce the block diagram of DianNao in Figure 3. The architecture contains buffers for caching input/output neurons and synapses, and a Neural Functional Unit (NFU) which is largely a pipelined version of the typical computations required to evaluate a neuron output: the multiplication of synaptic values by input neurons values in the first stage, additions of all these products in the second stage (adder trees), and application of a transfer function in the third stage (realized through linear interpolation). Depending on the layer type (classifier, convolution, pooling), different computational operators are invoked in each stage.

In order to compare their architecture against GPU, we reimplement a cycle-level bit-level version of DianNao, and we use the memory latency parameters mentioned in their article. For the sake of comparison, we use at least some (4) of the same layers (CONV2, CONV4\*, POOL1 and POOL2 respectively correspond to their CONV1, CONV5\*, POOL1, POOL3; the layer numbers are different but the notations are

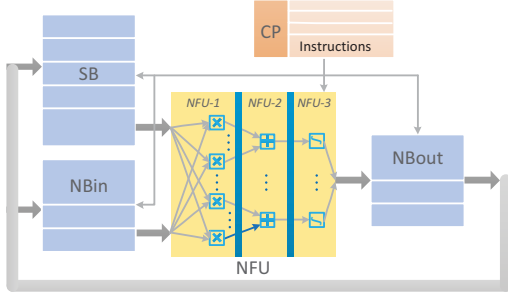


Figure 3: Block diagram of the DianNao accelerator [5].

the same), but we introduced even larger classifier layers (CLASS1 and CLASS2); CONV1 and CONV3\* are large convolutional layers with respectively shared and private kernels, more closely matching the ones used in the references cited in Table I. Since DianNao did not yet support LRN layers [5], we omit them from this comparison. In Figure 2, we report the speedup of our GPU implementation (NVIDIA K20M) over DianNao. We can observe that DianNao can achieve about 47.91% of the GPU performance on average, in 0.53% of the area (the K20M is 561 mm<sup>2</sup> at 28nm), which is a testimony to the potential efficiency of custom architectures.

However, the main limitation, acknowledged by the authors, is the memory bandwidth requirements of two important layer types: convolutional layers with private kernels (used in DNNs) and classifier layers used in both CNNs and DNNs. For these types of layers, the total number of required synapses can be massive, in the millions of parameters, or even tens or hundreds thereof. For an NFU processing 16 inputs of 16 output neurons (i.e., 256 synapses) per cycle, at 0.98GHz a peak bandwidth of 467.30 GB/s would be necessary. As a reference, the NVIDIA K20M GPU has 320-bit memory interfaces at 2.6 GHz which can operate on every half-clock, for a total of 208 GB/s. Chen et al. [5] also report that off-chip memory accesses increase the total energy cost by a factor of approximately 10x.

In the next section, we propose a custom node and multi-chip architecture to overcome this limitation.

## V. A MACHINE-LEARNING SUPERCOMPUTER

We call the proposed architecture a “supercomputer” because its goal is to achieve high sustained machine-learning performance, significantly beyond single-GPU performance, and because this capability is achieved using a multi-chip system. Still, each node is significantly cheaper than a typical GPU while exhibiting a comparable or higher compute density (number of operations per second divided by the area).

We design the architecture around the central property, specific to DNNs and CNNs, that the total memory footprint of their parameters, while large (up to tens of GB), can be

fully mapped to on-chip storage in a multi-chip system with a reasonable number of chips.

### A. Overview

As explained in Section IV, the fundamental issue is the memory storage (for reuse) or bandwidth requirements (for fetching) of the synapses of two types of layers: convolutional layers with private kernels (the most frequent case in DNNs), and classifier layers (which are usually fully connected, and thus have lots of synapses). We tackle this issue by adopting the following design principles: (1) we create an architecture where synapses are always stored close to the neurons which will use them, minimizing data movement, saving both time and energy; the architecture is fully distributed, there is no main memory; (2) we create an asymmetric architecture where each node footprint is massively biased towards storage rather than computations; (3) we transfer neurons values rather than synapses values because the former are orders of magnitude fewer than the latter in the aforementioned layers, requiring comparatively little external (across chips) bandwidth; (4) we enable high internal bandwidth by breaking down the local storage into many tiles.

The general architecture is a set of nodes, one per chip, all identical, arranged in a classic mesh topology. Each node contains significant storage, especially for synapses, and neural computational units (the classic pipeline of multipliers, adder trees and non-linear transfer functions implemented via linear interpolation), which we also call NFU for the sake of consistency with prior art, though our NFU is significantly more complex than the one proposed by Chen et al. [5] because its pipelined can be reconfigured for each layer and inference/training, see Section V-B3.

In the next subsections, we detail each component and we explain the rationale for the design choices.

*Driving example.* We use the classifier layer as a driving example because it is both challenging due to its large number of synapses, but also structurally simple, and thus adequate as a driving example; note that for the sake of completeness, we explain in Section V-B3 how all layers are implemented on the architecture. As explained in Section II, in a classifier layer, the  $N_o$  outputs are typically connected to all the  $N_i$  inputs, with one synaptic weight per connection. In terms of locality, it means that each input is reused  $N_o$  times, and that the synaptic weights are not reused within one classifier layer execution.

### B. Node

In this section, we present the architecture node and explain the rationale for its design.

1) *Synapses Close to Neurons:* One of the fundamental design characteristic of the proposed architecture is to locate the storage for synapses close to neurons and to make it massive. This design choice is motivated by the decision to

move only neurons and to keep synapses in a fixed storage location. This serves two purposes.

First, the architecture is targeted for both inference and training. In inference, the neurons of the previous layer are the inputs of the computation; in training, the neurons are forward-propagated (so neurons of the previous layer are the inputs) and then backward-propagated (so neurons of the *next* layer are now the inputs). As a result, depending on how data (neurons and synapses) are allocated to nodes, they need to be moved between the forward and backward phases. Since there are many more synapses than neurons (e.g.,  $O(N^2)$  vs.  $O(N)$  for classifier layers,  $K \times K \times N_{if} \times N_{of} \times N_x \times N_y$  vs.  $N_{if} \times N_x \times N_y$  for convolutional layers with private kernels, see Section II), it is only logical to move neuron outputs instead of synapses. Second, having all synapses (most of the computation inputs) next to computational operators provides low-energy/low-latency data (synapses) transfers and high internal bandwidth.

As shown in Table I, layer sizes can range from less than 1MB to about 1GB, most of them ranging in the tens of MB. While SRAMs are appropriate for caching purposes, they are not dense enough for such large-scale storage. However, eDRAMs are known to have a higher storage density. For instance, a 10MB SRAM memory requires  $20.73\text{mm}^2$  at 28nm [36], while an eDRAM memory of the same size and at the same technology node requires  $7.27\text{mm}^2$  [50], i.e., a 2.85x higher storage density.

Moreover, providing sufficient eDRAM capacity to hold all synapses on the combined eDRAM of all chips will save on off-chip DRAM accesses, which are particularly costly energy-wise. For instance, a read access to a 256-bit wide eDRAM array at 28nm consumes  $0.0192\text{nJ}$  ( $50\mu\text{A}$ ,  $0.9\text{V}$ ,  $606\text{ MHz}$ ) [25], while a 256-bit read access to a Micron DDR3 DRAM consumes  $6.18\text{nJ}$  at 28nm [40], i.e., an energy ratio of 321x. The ratio is largely due to the memory controller, the DDR3 physical-level interface, on-chip bus access, page activation, etc.

If the NFU is no longer limited by the memory bandwidth, it is possible to scale up its size in order to process more output neurons ( $N_o$ ) and more inputs per output neuron ( $N_i$ ) simultaneously, and thus, to improve the overall node throughput. For instance, to scale up by 16x the number of operations performed every cycle compared to the accelerator mentioned in Section IV, we need to have  $N_i = 64$  (instead of 16) and  $N_o = 64$  (instead of 16). In order to achieve maximal throughput, we must fetch  $N_i \times N_o$  16-bit values from the eDRAM to the NFU every cycle, i.e.,  $64 \times 64 \times 16 = 65536$  bits in this case.

However eDRAM has three well-known drawbacks: higher latency than SRAM, destructive reads and periodic refresh [38], as in traditional DRAMs. In order to compensate for the eDRAM drawbacks and still feed the NFU every cycle, we split the eDRAM into four banks (65536-bit wide in the

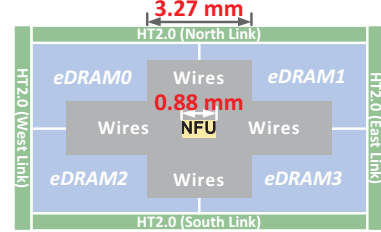


Figure 4: Simplified floorplan with a single central NFU showing wire congestion.

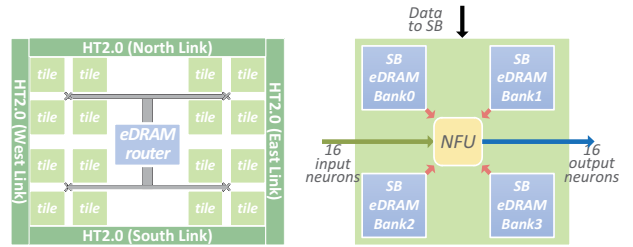


Figure 5: Tile-based organization of a node (left) and tile architecture (right). A node contains 16 tiles, two central eDRAM banks and fat tree interconnect; a tile has an NFU, four eDRAM banks and input/output interfaces to/from the central eDRAM banks.

above example), and we interleave the synapses rows among the four banks.

We placed and routed this design at 28nm (ST technology, LP), and we obtained the floorplan of Figure 4. The NFU footprint is very small at  $0.78\text{mm}^2$  ( $0.88\text{mm} \times 0.88\text{mm}$ ), but the process imposes an average spacing of  $0.2\mu\text{m}$  between wires, and provides only 4 horizontal metal layers. As a result, the 65536 wires connecting the NFU to the eDRAM require a width of  $\frac{65536 \times 0.2}{4} = 3.2768\text{mm}$ , see Figure 4. Consequently, wires occupy  $4 \times 3.2768 \times 3.2768 - 0.88 \times 0.88 = 42.18\text{mm}^2$ , which is almost equal to the combined area of all eDRAM banks, all NFUs and the I/O.

2) *High Internal Bandwidth*: In order to avoid this congestion, we adopt a tile-based design, as shown in Figure 5. The output neurons are spread out in the different tiles, so that each NFU can simultaneously process 16 input neurons

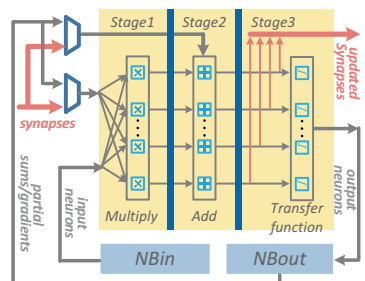


Figure 6: The different (parallel) operators of an NFU: multipliers, adders, max, transfer function.

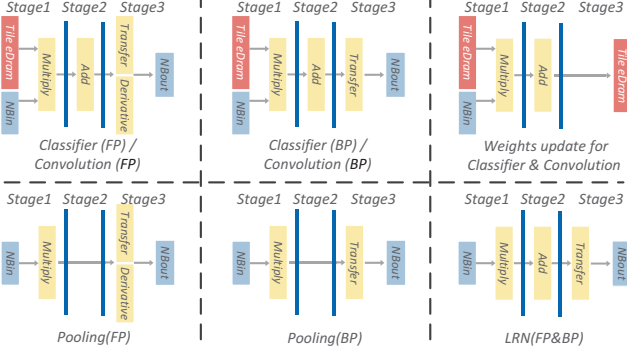


Figure 7: Different pipeline configurations for CONV, LRN, POOL and CLASS layers.

of 16 output neurons (256 parallel operations), see Figure 6. As a result, the NFU in each tile is significantly smaller, and only  $16 \times 16 \times 16 = 4096$  bits must be extracted each cycle from the eDRAM. We keep the 4-bank (4096-bit wide banks) organization to compensate for the aforementioned eDRAM weaknesses, and we obtain the tile design of Figure 5. We placed and routed one such tile, and obtained an area of  $1.89 \text{ mm}^2$ , so that 16 such tiles account for  $30.16 \text{ mm}^2$ , i.e., a 28.5% area reduction over the previous design, because the routing network now only accounts for 8.97% of the overall area.

All the tiles are connected through a fat tree which serves to broadcast the input neurons values to each tile, and to collect the output neurons values from each tile. At the center of the chip, there are two special eDRAM banks, one for input neurons, the other for output neurons. It is important to understand that, even with a large number of tiles and chips, the total number of *hardware* output neurons of all NFUs, can still be small compared to the actual number of neurons found in large layers. As a result, for each set of input neurons broadcasted to all tiles, multiple different output neurons are being computed on the same hardware neuron. The intermediate values of these neurons are saved back locally in the tile eDRAM. When the computation of an output neuron is finished (all input neurons have been factored in), the value is sent through the fat tree to the center of the chip to the corresponding (output neurons) central eDRAM bank.

3) *Configurability (Layers, Inference vs. Training)*: We can adapt the tile, and the NFU pipeline in particular, to the different layers and the execution mode (inference or training). The NFU is decomposed into a number of hardware blocks: adder block (which can be configured either as a 256-input, 16-output adder tree, or 256 parallel adders), multiplier block (256 parallel multipliers), max block (16 parallel max operations), and transfer block (two independent sub-blocks performing 16 piecewise linear interpolations; the  $a, b$  linear interpolation coefficients, i.e.,  $y = a \times x + b$ , for each block are stored in two 16-

entry SRAMs and can be configured to implement any transfer function and its derivative). In Figure 7, we show the different pipeline configurations for CONV, LRN, POOL and CLASS layers in the forward and backward phases.

Inference	Training	Error
Floating-Point	Floating-Point	0.82%
Fixed-Point (16 bits)	Floating-Point	0.83%
Fixed-Point (32 bits)	Floating-Point	0.83%
Fixed-Point (16 bits)	Fixed-Point (16 bits)	(no convergence)
Fixed-Point (16 bits)	Fixed-Point (32 bits)	0.91%

Table II: Impact of fixed-point computations on error.

Each hardware block is designed to allow the aggregation of 16-bit operators (adders, multipliers, max, and the adders/multipliers used for linear interpolation) into fewer 32-bit operators (two 16-bit adders into one 32-bit adder, four 16-bit multipliers into 32-bit multiplier, two 16-bit max into one 32-bit max); the overhead cost of aggregable operators is very low [26]. While 16-bit operators are largely sufficient for the inference usage, they may either reduce the accuracy and/or increase (or even prevent) the convergence of training. As an example, consider a CNN trained on MNIST [35] using various combinations of fixed and floating-point representations. There is almost no impact on error if 16-bit fixed-point is used in inference only, but there is no convergence if it is used also for training. On the other hand, there is only a small impact on error if 32-bit fixed-point is used: 0.91% instead of 0.83%; moreover, in further tests, we note that the error obtained for 28 bits is 1.72%, so it decreases rapidly to 0.91% by adding 4 more bits, and further aggregating operators allows to further decrease the fixed-point error. By default, we use 32-bit operators in training mode.

Beyond pipeline and block configurations, the tile must be configured for different data movement cases. For instance, a classifier layer input can come from the node central eDRAM (possibly after transfer from another node), or it can come from the two SRAM storages (16KB) which are used to buffer input and output neuron values, or even temporary values (such as neurons partial sums) to enable reuse of input neurons values) as proposed by Chen et al. [5]. In the backward phase, the NFU must also write to the tile eDRAM after the weights update step, see Figure 7. During the gradient computations step, the input and output gradients use the data paths of input and output neurons in the forward phase, see Figure 7 again.

### C. Interconnect

Because neurons are the only values transferred, and because these values are heavily reused within each node, the amount of communications, while significant, is not a bottleneck except for a few layers and many-node systems, as later discussed in Section VII. As a result, we did not develop a custom high-speed interconnect for our purpose,

we turned to commercially available high-performance interfaces, and we used a HyperTransport (HT) 2.0 IP block. The HT2.0 physical layer interface (PHY) we used for the 28nm process is a long thin strip of  $5.635\text{mm} \times 0.5575\text{mm}$  (with a protrusion) due to its usual location at the periphery of the die.

We use a simple 2D mesh topology; that choice may be later revisited in favor of a more efficient 3D mesh topology though. Because of the mesh topology of the architecture, each chip must connect to four neighbors via four HT2.0 IP blocks (see Figure 9), each with 16x HT links, i.e., 16 pairs of differential outgoing signals, and 16 pairs of differential incoming signals, at a frequency of 1.6GHz (we connect the HT to the central eDRAM through a 128-bit, 4-entry, asynchronous FIFO). Each HT block provides a bandwidth of 6.4GB/s in each direction. The HT2.0 latency between two neighbor nodes is about 80ns.

**Router.** Next to the central block of the tile, we implement the router, see Figure 5. We use wormhole routing, the router has five input/output ports (4 directions and injection/ejection port). Each input port contains 8 virtual channels (5 flit slots per VC). A 5x5 crossbar is equipped to connect all input/output ports. The router has four pipeline stages: routing computation (RC), VC allocation (VA), switch allocation (SA) and switch traversal (ST).

#### D. Overall Characteristics

Parameters	Settings	Parameters	Settings
Frequency	606MHz	tile eDRAM latency	$\sim 3$ cycles
# of tiles	16	central eDRAM size	4MB
# of 16-bit multipliers/tile	256+32	central eDRAM latency	$\sim 10$ cycles
# of 16-bit adders/tile	256+32	Link bandwidth	6.4x4GB/s
tile eDRAM size/tile	2MB	Link latency	80ns

Table III: Architecture characteristics.

The architecture characteristics are summarized in Table III. We have implemented 16 tiles per node. In each tile, each of the 4 eDRAM banks contains 1024 rows of 4096 bits. The total eDRAM capacity in one tile is thus  $4 \times 1024 \times 4096 = 2\text{MB}$ . The central eDRAM in each node has a size of 4MB. The total node eDRAM capacity is thus  $16 \times 2 + 4 = 36\text{MB}$ .

In order to avoid the circuit and time overhead of asynchronous transfers, we decided to clock the NFU at the same frequency as the eDRAM available in the 28nm technology we used, i.e., 606MHz. Note that the NFU implemented by Chen et al. [5] was clocked at 0.98GHz at 65nm, so our decision is very conservative considering we use a 28nm technology. We leave the implementation of a faster NFU and asynchronous communications with eDRAM for future work. Nonetheless, a node still has a peak performance of  $16 \times (288+288) \times 606 = 5.58$  TeraOps/s for 16-bit operation. For 32-bit operation, the peak performance of a node is  $16 \times (144 + 72) \times 606 = 2.09$  TeraOps/s due to operator aggregation, see Section V-B3.

Inst Name	CP	central eDRAM	SB	NBin	NBout	NFU
	READ OP					
	WRITE OP					
	READ ADDR					
	WRITE ADDR					
	READ STRIDE					
	WRITE STRIDE					
	READ ITER					
	WRITE ITER					

Table IV: Node instruction format.

CP	central eDRAM	SB	NBin	NBout	NFU
LOAD LOAD LOAD					
STORE WRITE WRITE WRITE					
192 128 64 0					
256 256 256 256					
0 0 0 0					
4 4 4 4					
64 64 64 64					
4 4 4 4					
NULL NULL NULL NULL					
768 512 256 0					
1 1 1 1					
READ READ READ READ					
NULL NULL NULL NULL					
0 0 0 0					
1 1 1 1					
READ READ READ READ					
NULL NULL NULL NULL					
0 0 0 0					
1 1 1 1					
READ READ READ READ					
NULL NULL NULL NULL					
0 0 0 0					
MUL MUL MUL MUL					
ADD ADD ADD ADD					
SIGNMOP NULL NULL NULL					
1 1 1 1					
0 0 0 0					

Table V: An example of classifier code ( $N_i = 4096$ ,  $N_o = 4096$ , 4 nodes).

#### E. Programming, Code Generation and Multi-Node Mapping

##### 1) Programming, Control and Code Generation:

This architecture can be viewed as a system ASIC, so the programming requirements are low, the architecture essentially has to be configured and the input data is fed in. The input data (values of the input layer) is initially partitioned across nodes and stored in a central eDRAM bank. The neural network configuration is implemented in the form of a sequence of *node* instructions, one sequence per node, produced by a code generator. An example output of the code generator for the inference phase of the CLASS2 layer is shown in Table V.

In this example, output neurons are partitioned into multiple 256-bit data blocks, where each block contains  $256/16 = 16$  neurons. Each node is allocated  $4096/16/4 = 64$  output data blocks (and it stores a quarter of all input neurons, i.e.,  $4096/4 = 1024$ ), and each tile is allocated  $64/16 = 4$  output data blocks, resulting in 4 instructions per node. An instruction will load 128 input data blocks from the central eDRAM to the tiles. In the first three instructions, all the tiles will get the same input neurons, and read synaptic weights from their local (tile) eDRAM, then write back the partial sums (of output neurons) to their local NBout SRAM. In the last instruction, the NFU in each tile will finalize the sums, apply the transfer function, and store the output values back to the central eDRAM.

These node instructions themselves drive the control of each tile; the control circuit of each node generates tile instructions and sends them to each tile. The spirit of a node or tile instruction is to perform the same layer computations (e.g., multiply-add-transf for classifier layers) on a set of contiguous input data (input neurons in the forward phase, output neurons, gradients or synapses in the backward phase). The fact the data of one instruction is contiguous allows to characterize it with only three operands: start address, step and number of iterations.

The control provides two modes of operations: processing one row at a time or *batch learning* [48], where multiple

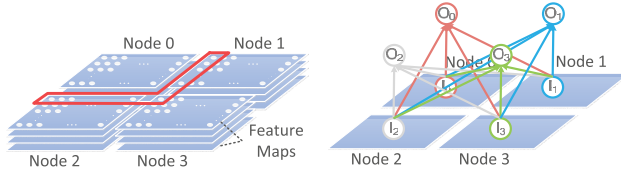


Figure 8: Mapping of (left) a convolutional (or pooling) layer with 4 feature maps; the red section indicates the input neurons used by node 0; (right) a classifier layer.

rows are processed at the same time, i.e., multiple instances of the same layer are evaluated simultaneously, albeit for different input data. This method is commonly used in machine-learning for a more stable gradient descent, and it also has the benefit of improving synapses reuse, at the cost of slower convergence and a larger memory capacity (since multiple instances of inputs/outputs must be stored).

2) *Multi-Node Mapping*: At the end of a layer, each node contains a set of output neurons values, which have been stored back in the central eDRAM, see Figure 5. These output neurons form the input neurons of the next layer; so, implicitly, at the beginning of a layer, the input neurons are distributed across all nodes, in the form of 3D rectangles corresponding to all feature maps of a subset of a layer, see Figure 8. These input neurons will be first distributed to all node tiles through the (fat tree) internal network, see Figure 5. Simultaneously, the node control starts to send the block of input neurons to the rest of the nodes through the mesh.

With respect to communications, there are three main layer cases to consider. First, convolutional and pooling layers are characterized by local connectivity defined by the small window (convolutional or pooling kernel) used to sample the input neurons. Due to the local connectivity, the amount of inter-node communications is very low (most communications are intra-node), mostly occurring at the border of the layer rectangle mapped to each node, see Figure 8.

For local response normalization layers, since all feature maps at a given location are always mapped to the same node, there is no inter-node communication.

Finally, communications can be high for classifier layers because each output neuron uses all input neurons, see Figure 8. At the same time, the communication pattern is simple, equivalent to a broadcast. Since each node performs roughly the same amount of computations at the same speed, and since each node must simultaneously broadcast its set of input neurons to all other nodes, we adopt a computing-and-forwarding communication scheme [24], which is equivalent to arranging the nodes communications according to a regular ring pattern. A node can start processing the newly arrived block of input neurons as soon as it has finished its own computations, and has sent the previous block of input neurons; so the decision is made *locally*, there is no *global*

*synchronization or barrier*.

## VI. METHODOLOGY

### A. Measurements

Our experiments use the following three tools.

**CAD tools.** We implemented a Verilog version of the node, then synthesized it, and did the layout. The area, energy and critical path delays are obtained after layout using the ST 28nm Low Power (LP) technology (0.9V). We used the Synopsys Design Compiler for the synthesis, ICC Compiler for the layout, and the power consumption was estimated using Synopsys PrimeTime PX.

**Time, eDRAM and inter-node measurements.** We use VCS to simulate the node RTL, an eDRAM model which includes destructive reads, and periodic refresh of a banked eDRAM running at 606MHz (the eDRAM energy was collected using CACTI5.3 [1] after integrating the 1T1C cell characteristics at 28nm [25]), and inter-node communications were simulated using the cycle-level Booksim2.0 interconnection network simulator [10] (Orion2.0 [29] for the network energy model).

**GPU.** We use the NVIDIA K20M GPU of Section III as a baseline. The GPU can also report its power usage. We use CUDA SDK 5.5 to compile the CUDA version of neural network codes.

### B. Baseline

In order to maximize the quality of our baseline, we extracted the CUDA versions from a tuned open-source version, CUDA Convnet [31]. In order to assess the quality of this baseline, we have compared it against the C++ version run on the Intel SIMD CPU, see Section III. For the C++ version, we have first compared the SIMD version against a non-SIMD version (SIMD compilation deactivated), and we have observed an average speedup of the SIMD version of 4.07x, confirming that the compiler was effectively taking advantage of the SIMD unit. As mentioned in Section III, the CUDA/GPU over the C++/CPU (SIMD) speedups reported in Figure 2 are in line with some of the best reported results so far, by Ciresan et al. [7] (10x to 60x).

## VII. EXPERIMENTAL RESULTS

We first present the main characteristics of the node layout, then present the performance and energy results of the multi-chip system.

### A. Main Characteristics

The cell-based layout of the chip is shown in Figure 9, and the area breakdown in Table VI. 44.53% of the chip area is used by the 16 tiles, 26.02% by the four HT IPs, 11.66% by the central block (including 4MB eDRAM, router and control logic). The wires between the central block and the tiles occupy 8.97% of the area. Overall, about a half (47.55%) of the chip is consumed by memory cells (mostly

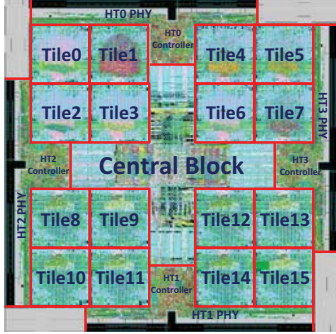


Figure 9: Snapshot of the node layout.

Component/Block	Area ( $\mu\text{m}^2$ )	(%)	Power (W)	(%)
WHOLE CHIP	67,732,900		15.97	
Central Block	7,898,081	(11.66%)	1.80	(11.27%)
Tiles	30,161,968	(44.53%)	6.15	(38.53%)
HT's	17,620,440	(26.02%)	8.01	(50.14%)
Wires	6,078,608	(8.97%)	0.01	(0.06%)
Other	5,973,803	(8.82%)		
Combinational	3,979,345	(5.88%)	6.06	(37.97%)
Memory	32207390	(47.55%)	6.12	(38.30%)
Registers	3,348,677	(4.94%)	3.07	(19.25%)
Clock network	586323	(0.87%)	0.71	(4.48%)
Filler cell	27,611,165	(40.76%)		

Table VI: Node layout characteristics.

eDRAM). The combinational logic and register only account for 5.88% and 4.94% of the area respectively.

We used Synopsys PrimePower to estimate the power consumption of the chip. The peak power consumption is 15.97 W (at a pessimistic 100% toggle rate), i.e., roughly 5–10% of a state-of-the-art GPU card. The architecture block breakdown shows that the tiles consume more than one third (38.53%) of the power, and the four HT IPs consume about one half (50.14%). The component breakdown shows that, overall, memory cells (tile eDRAMs + central eDRAM) account for 38.30% of the total power, combinational logic and registers (mostly NFUs and HT protocol analyzers) consume 37.97% and 19.25% respectively.

### B. Performance

In Figure 10, we compare the performance of our architecture against the GPU baseline described in Section VI. Because of its large memory footprint (numbers of neurons and synapses), CONV1 needs a 4-node system. Even though CONV1 is a shared-kernel convolutional layer, it contains 256 input feature maps, 384 output feature maps and  $11 \times 11$  kernels, so that the total number of synapses is  $256 \times 384 \times 11 \times 11 = 11,894,784$ , i.e., 22.69 MB (16-bit data). We must also store all layer inputs and outputs, i.e., respectively  $256 \times 256 \times 256 \times 2 = 32\text{MB}$ ,  $246 \times 246 \times 384 \times 2 = 44.32\text{MB}$  (fewer output neurons due to a border effect since the kernel is  $11 \times 11$ ). So, overall, 99.01MB must be stored, which exceeds the node capacity of 36MB. The convolutional layers with private kernels, i.e.,

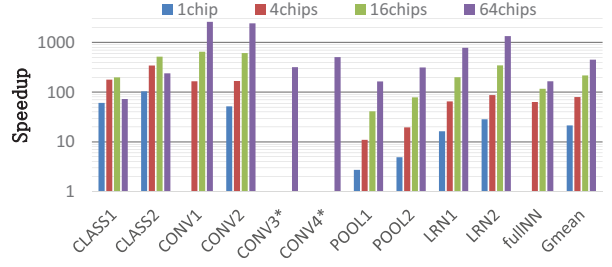


Figure 10: Speedup w.r.t. the GPU baseline (inference). Note that CONV1 and the full NN need a 4-node system, while CONV3\* and CONV4\* even need a 36-node system.

CONV3\* and CONV4\*, need a 36-node system because their size is respectively 1.29 GB and 1.32 GB. The full NN contains 59.48M synapses, i.e., 118.96MB (16-bit data), requiring at least 4 nodes.

On average, the 1-node, 4-node, 16-node and 64-node architectures are respectively 21.38x, 79.81x, 216.72x, and 450.65x faster than the GPU baseline.<sup>1</sup> The first reason for the higher performance is the large number of operators: in each node, there are 9216 operators (mostly multipliers and adders), compared to the 2496 MACs of the GPU. The second reason is that the on-chip eDRAM provides the necessary bandwidth and low-latency access to feed these many operators.

Nevertheless, the scalability of the different layers varies a lot. LRN layers scale the best (no inter-node communication) with a speedup of up to 1340.77x for 64 nodes (LRN2), CONV and POOL layers scale almost as well because they only have inter-node communications on border elements, e.g., CONV1 achieves a speedup of 2595.23x for 64 nodes, but the actual speedup of LRN and POOL layers is lower than CONV layers because they are less computationally intensive. On the other hand, CLASS layers scale less well because of the high amount of inter-node communications, since each output neuron uses all input neurons from different nodes, see Section V-E2, e.g., CLASS1 has a speedup of 72.96x for 64 nodes. This is further illustrated in the time breakdown of Figure 11. Note that each bar is normalized to the total execution time, but due to the overlap of computation and communication, the cumulated bars can exceed 100%. This communication issue is mostly due to our relatively simple 2D mesh topology where the larger the number of nodes, the longer the time required to send each block of inputs to all nodes. It is likely that a more sophisticated multi-dimensional torus topology [4] can largely reduce the total broadcast time as the number of nodes increases, but we leave this optimization for future work.

<sup>1</sup>Considering that the area of K20M GPU is about  $550 \text{ mm}^2$ , and our node is only  $67.7 \text{ mm}^2$ , our design also has a high area-normalized speedup with respect to GPU (21.38\*550/67.7 = 173.69x for 1-node and 450.65\*550/(64 \* 67.7) = 57.20x for 64-node).

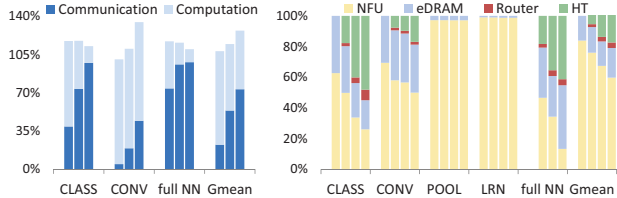


Figure 11: Time breakdown (left) for 4, 16 and 64 nodes, (right) breakdown for 1, 4, 16, 64 nodes; CLASS, CONV, POOL, LRN stand for the geometric means of all layers of the corresponding type, Gmean for the global geometric mean.

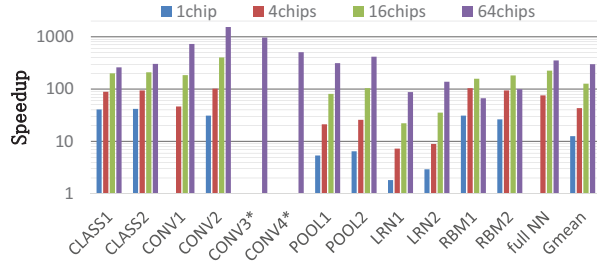


Figure 12: Speedup w.r.t. the GPU baseline (training).

Finally, we note that the full NN scales similarly to CLASS layers (63.35x, 116.85x, 164.80x for 4-node, 16-node, 64-node respectively). While it may suggest that CLASS layers dominate the full NN execution time, a breakdown by layer type, see Table VII, shows that it is not the case, on the contrary, CONV layers largely dominate. The reason is simply that this full NN contains layers which are a bit small for a large 64-node machine. For instance, there are three CONV layers with a dimension of 13x13 (though 256 to 384 feature maps), so, even though all feature maps are mapped to the same node, we need to attribute an  $X \times Y$  area of size  $2 \times 2$  or  $3 \times 3$  at most per node ( $\frac{13 \times 13}{64} = 2.69$ ) which means that either we do not use all nodes, or inter-node communications are required for every kernel computation.

	CONV	LRN	POOL	CLASS
4-node	96.63%	0.60%	0.47%	2.31%
16-node	96.87%	0.28%	0.22%	2.63%
64-node	92.25%	0.10%	0.08%	7.57%

Table VII: Full NN execution time breakdown per layer type.

**Training and initialization.** We carry out similar experiments for back propagation, and the weights pre-training phase (RBM) using 32-bit fixed point operators (while inference uses 16-bit fixed-point operators), see Section V-B3. On average, the 1-node, 4-node, 16-node and 64-node architectures are respectively 12.62x, 43.23x, 126.66x and 300.04x faster than the GPU baseline; the speedups are high though lower than for inference essentially because of operators aggregation. As shown in Figure 12, for CLASS

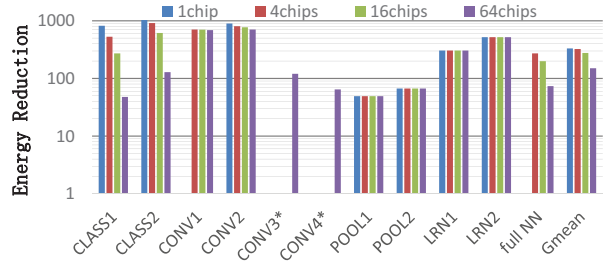


Figure 13: Energy reduction w.r.t. the GPU baseline (inference).

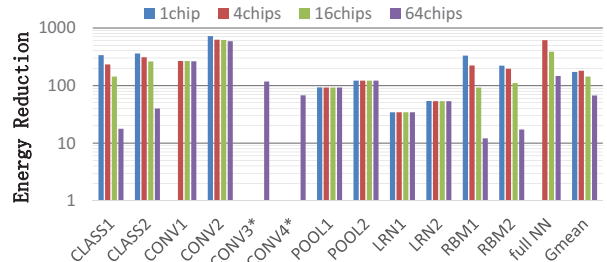


Figure 14: Energy reduction w.r.t. the GPU baseline (training).

layers, the scalability of the training phase is better than that of the inference phase, mainly thanks to CLASS layers which have almost double the amount of computations w.r.t. inference, for the same amount of communications. The scalability of RBM initializations is fairly similar to that of CLASS layers in the inference phase.

### C. Energy Consumption

As shown in Figure 13, the 1-node, 4-node, 16-node and 64-node architectures can reduce the energy by 330.56x, 323.74x, 276.04x, and 150.31x respectively compared to the GPU baseline. The minimum energy improvement is 47.66x for CLASS1 with 64 nodes, while the best energy improvement is 896.58x, achieved with CONV2 on a single node. For convolutional, pooling, and LRN layers, we observe that the energy benefit remains relatively stable as the number of nodes is scaled up, though it degrades for classifier layers. The latter is expected as the average communication (and thus overall execution) time increases; again, a multi-dimensional torus should help reduce this energy loss.

In the energy breakdown of Figure 11, we can observe that, for the 1-node architecture, about 83.89% of the energy is consumed by the NFU. As we scale up the number of nodes, the trend largely corroborates previous observations: the ratio of energy spent in HT progressively increases to 29.32% on average for a 64-node system, especially due to the larger number of communications in classifier layers (48.11%).

**Training and initialization.** For training and initialization, the energy reduction of our architecture with respect to the GPU baseline on training is also high: 172.39x, 180.42x,

142.59x, and 66.94x for the 1-node, 4-node, 16-node and 64-node architectures, see Figure 14. The scalability behavior is similar to that of the inference phase.

## VIII. RELATED WORK

**Machine-Learning.** Convolutional and Deep Neural Networks have become popular algorithms in data center based services: they are used for web search [27], image analysis [41], speech recognition [9], etc. Such services are computationally intensive, and considering the energy and operating costs of data centers, custom architectures could help from both a performance and energy perspective. But web services are only the most visible applications. CNNs are being used for handwritten digits recognition [28] with applications in banking and post-offices, Dahl et al. [9] have recently won a pharmaceutical contest using DNN algorithms. More generally, such algorithms might take a central role in the so-called big data application domain. While CNNs and DNNs keep evolving, we note for instance that the first CNN design [35] still achieves very good results compared to the latest instantiations on benchmarks such as the MNIST handwritten digits [35], with a recognition accuracy of 1.7% (1998) versus 0.23% for the best algorithm by Ciresan et al. [6] (2012).

So, even though there is an inherent risk in freezing algorithms in hardware, (1) hardware can rapidly evolve with machine-learning progress, much like it currently (and rapidly) evolves with technology progress, (2) what machine-learning researchers rightfully view as significant accuracy progress from their perspective (e.g., improving accuracy by 1 or 2% can be very difficult) may not be so significant from an end-user perspective, so that hardware needs not implement and follow each and every evolution, (3) end users are already accustomed to the notion of software libraries, and they can always choose between a rigid but very fast “hardware library” and a slow but more flexible CPU/GPU implementation.

**Custom accelerators.** Due to the end of Dennard scaling and the notion of Dark Silicon [42], [15], architecture customization is increasingly viewed as one of the most promising paths forward. So far, the emphasis has been especially on custom *accelerators*, i.e., custom tiles within a heterogeneous multi-cores. Accelerators for video compression [21], image convolutions [44], libraries or specific workloads [49], [17] have been proposed.

Closer to the target algorithms of this paper, a number of studies have recently advocated the notion of neural network accelerators, either to approximate any function of a program [16], for signal-processing tasks [2] or specifically for machine-learning tasks [22], [23], [47], [5].

**Large-Scale custom architectures.** There are few examples of custom architectures targeting large-scale neural networks. The closest examples are the following. Schemmel

et al. [46] propose a wafer-scale design capable of implementing thousands of neurons and millions of synapses. Khan et al. [30] propose the SpiNNaker system, which is a multi-chip supercomputer where each node contains 20+ ARM9 cores linked by an asynchronous network; the planned target is a million-core machine capable of modeling a billion neurons. Finally, the IBM Cognitive Chip [39] is a functional chip capable of implementing 256 neurons and 256K synapses in 4mm<sup>2</sup> at 45nm. However, the common point between these different architectures is that their goal is the emulation of *biological neurons*, not machine-learning tasks, even though some of them have demonstrated machine-learning capabilities on simple tasks. Moreover, the neurons they implement are inspired from biology, i.e., spiking neurons, they do not implement the CNNs and DNNs which are the focus of our architecture. Majumdar et al. [37] investigate a parallel architecture for various machine-learning algorithms, including, but not only, neural networks; unlike our architecture, they have an off-chip banked memory, and they introduce memory banks close to PEs (similar to those found in GPUs) for caching purposes. Finally, beyond neural networks and machine-learning tasks, other large-scale custom architectures have been proposed, such as the recently proposed Anton [12], for molecular dynamics simulation.

## IX. CONCLUSIONS AND FUTURE WORK

In this article, we investigate a custom multi-chip architecture for state-of-the-art machine-learning algorithms (CNNs and DNNs), motivated by the increasingly central role of such algorithms in large-scale deployments of sophisticated services for consumers and industry. On both GPUs and recently proposed accelerators, such algorithms exhibit good speedups and area savings respectively, but they remain largely bandwidth-limited. We show that it is possible to design a multi-chip architecture which can outperform a single GPU by up to 450.65x and reduce energy by up to 150.31x using 64 nodes. Each node has an area of 67.73mm<sup>2</sup> at 28nm.

We plan to improve this architecture along several directions: increasing the clock frequency of the NFU, multi-dimensional torus interconnects to improve the scalability of large classifier layers, investigating more flexible control in the form of a simple VLIW core per node and the associated toolchain. A tape-out of a node chip is planned soon, followed by a multi-node prototype.

## ACKNOWLEDGMENTS

This work is partially supported by the NSF of China (under Grants 61100163, 61133004, 61222204, 61221062, 61303158, 61432016, 61472396, 61473275), the 863 Program of China (under Grant 2012AA012202), the 973 Program of China (under Grant 2011CB302500), the Strategic Priority Research Program of the CAS (under Grant

XDA06010403), the International Collaboration Key Program of the CAS (under Grant 171111KYSB20130002), a Google Faculty Research Award, the Intel Collaborative Research Institute for Computational Intelligence (ICRI-CI), the 10,000 talent program, and the 1,000 talent program.

## REFERENCES

- [1] Cacti 5.3, <http://quid.hpl.hp.com:9081/cacti/>.
- [2] B. Belhadj, A. Joubert, Z. Li, R. Heliot, and O. Temam. Continuous Real-World Inputs Can Open Up Alternative Accelerator Designs. In *International Symposium on Computer Architecture*, 2013.
- [3] C. Bienia, S. Kumar, J. P. Singh, and K. Li. The PARSEC benchmark suite: Characterization and architectural implications. In *International Conference on Parallel Architectures and Compilation Techniques*, New York, New York, USA, 2008. ACM Press.
- [4] D. Chen, N. Eisley, P. Heidelberger, R. Senger, Y. Sugawara, S. Kumar, V. Salapura, D. Satterfield, B. Steinmacher-Burow, and J. Parker. The ibm blue gene/q interconnection fabric. In *IEEE Micro*, 2012.
- [5] T. Chen, Z. Du, N. Sun, J. Wang, C. Wu, Y. Chen, and O. Temam. DianNao: A Small-Footprint High-Throughput Accelerator for Ubiquitous Machine-Learning. In *International Conference on Architectural Support for Programming Languages and Operating Systems*, 2014.
- [6] D. Cirean, U. Meier, and J. Schmidhuber. Multi-column Deep Neural Networks for Image Classification. In *International Conference of Pattern Recognition*, pages 3642–3649, 2012.
- [7] D. Ciresan, U. Meier, and J. Masci. Flexible, high performance convolutional neural networks for image classification. *International Joint Conference on Artificial Intelligence*, pages 1237–1242, 2011.
- [8] A. Coates, B. Huval, T. Wang, D. J. Wu, and A. Y. Ng. Deep learning with cots hpc systems. In *International Conference on Machine Learning*, 2013.
- [9] G. Dahl, T. Sainath, and G. Hinton. Improving Deep Neural Networks for LVCSR using Rectified Linear Units and Dropout. In *International Conference on Acoustics, Speech and Signal Processing*, 2013.
- [10] W. Dally and B. Towles. *Principles and Practices of Interconnection Networks*. Morgan Kaufmann Publishers Inc., San Francisco, CA, USA, 2003.
- [11] J. Dean, G. S. Corrado, R. Monga, K. Chen, M. Devin, Q. V. Le, M. Z. Mao, M. Ranzato, A. Senior, P. Tucker, K. Yang, and A. Y. Ng. Large scale distributed deep networks. In *Annual Conference on Neural Information Processing Systems (NIPS)*, 2012.
- [12] M. M. Deneroff, D. E. Shaw, R. O. Dror, J. S. Kuskin, R. H. Larson, J. K. Salmon, and C. Young. A specialized asic for molecular dynamics. In *Hot Chips*, 2008.
- [13] J. Deng, W. Dong, R. Socher, L.-J. Li, K. Li, and L. Fei-Fei. ImageNet: A large-scale hierarchical image database. In *Conference on Computer Vision and Pattern Recognition*, 2009.
- [14] P. Dubey. Recognition, Mining and Synthesis Moves Computers to the Era of Tera. *Technology@Intel Magazine*, 9(2):1–10, 2005.
- [15] H. Esmaeilzadeh, E. Blehm, R. S. Amant, K. Sankaralingam, and D. Burger. Dark Silicon and the End of Multicore Scaling. In *Proceedings of the 38th International Symposium on Computer Architecture (ISCA)*, June 2011.
- [16] H. Esmaeilzadeh, A. Sampson, L. Ceze, and D. Burger. Neural Acceleration for General-Purpose Approximate Programs. In *International Symposium on Microarchitecture*, number 3, pages 1–6, 2012.
- [17] K. Fan, M. Kudlur, G. S. Dasika, and S. A. Mahlke. Bridging the computation gap between programmable processors and hardwired accelerators. In *HPCA*, pages 313–322. IEEE Computer Society, 2009.
- [18] C. Farabet, B. Martini, B. Corda, P. Akselrod, E. Culurciello, and Y. LeCun. NeuFlow: A runtime reconfigurable dataflow processor for vision. In *CVPR Workshop*, pages 109–116. Ieee, June 2011.
- [19] D. A. Ferrucci. Introduction to "This is Watson". *IBM Journal of Research and Development*, 56:1:1–1:15, 2012.
- [20] R. Hadsell, P. Serbanet, J. Ben, A. Erkan, M. Scoffier, K. Kavukcuoglu, U. Muller, and Y. LeCun. Learning long-range vision for autonomous off-road driving. *Journal of Field Robotics*, 26:120–144, 2009.
- [21] R. Hameed, W. Qadeer, M. Wachs, O. Azizi, A. Solomatnikov, B. C. Lee, S. Richardson, C. Kozyrakis, and M. Horowitz. Understanding sources of inefficiency in general-purpose chips. In *International Symposium on Computer Architecture*, page 37, New York, New York, USA, 2010. ACM Press.
- [22] A. Hashmi, H. Berry, O. Temam, and M. Lipasti. Automatic Abstraction and Fault Tolerance in Cortical Microarchitectures. In *International Symposium on Computer architecture*, New York, NY, 2011. ACM.
- [23] A. Hashmi, A. Nere, J. J. Thomas, and M. Lipasti. A case for neuromorphic ISAs. In *International Conference on Architectural Support for Programming Languages and Operating Systems*, New York, NY, 2011. ACM.
- [24] S.-N. Hong and G. Caire. Compute-and-forward strategies for cooperative distributed antenna systems. In *IEEE Transactions on Information Theory*, 2013.
- [25] K. Huang, Y. Ting, C. Chang, K. Tu, K. Tzeng, H. Chu, C. Pai, A. Katoch, W. Kuo, K. Chen, T. Hsieh, C. Tsai, W. Chiang, H. Lee, A. Achyuthan, C. Chen, H. Chin, M. Wang, C. Wang, C. Tsai, C. Oconnell, S. Natarajan, S. Wu, I. Wang, H. Hwang, and L. Tran. A high-performance, high-density 28nm edram technology with high-k/metal-gate. In *IEEE International Electron Devices Meeting (IEDM)*, 2011.
- [26] L. Huang, S. Ma, L. Shen, Z. Wang, and N. Xiao. Low-cost binary128 floating-point FMA unit design with SIMD support. *IEEE Transactions on Computers*, 61:745–751, 2012.
- [27] P. Huang, X. He, J. Gao, and L. Deng. Learning deep structured semantic models for web search using clickthrough data. In *International Conference on Information and Knowledge Management*, 2013.

- [28] K. Jarrett, K. Kavukcuoglu, M. Ranzato, and Y. LeCun. What is the best multi-stage architecture for object recognition? In *Computer Vision, 2009 ...*, pages 2146–2153. Ieee, Sept. 2009.
- [29] A. Kahng, B. Li, L.-S. Peh, and K. Samadi. Orion 2.0: A power-area simulator for interconnection networks. In *IEEE Transactions on Very Large Scale Integration Systems*, 2012.
- [30] M. M. Khan, D. R. Lester, L. A. Plana, A. Rast, X. Jin, E. Painkras, and S. B. Furber. SpiNNaker: Mapping neural networks onto a massively-parallel chip multiprocessor. In *IEEE International Joint Conference on Neural Networks (IJCNN)*, pages 2849–2856. Ieee, 2008.
- [31] A. Krizhevsky. <https://code.google.com/p/cuda-convnet/>.
- [32] A. Krizhevsky, I. Sutskever, and G. Hinton. Imagenet classification with deep convolutional neural networks. In *Advances in Neural Information Processing Systems*, pages 1–9, 2012.
- [33] H. Larochelle, D. Erhan, A. Courville, J. Bergstra, and Y. Bengio. An empirical evaluation of deep architectures on problems with many factors of variation. In *International Conference on Machine Learning*, pages 473–480, New York, New York, USA, 2007. ACM Press.
- [34] Q. V. Le, M. A. Ranzato, R. Monga, M. Devin, K. Chen, G. S. Corrado, J. Dean, and A. Y. Ng. Building High-level Features Using Large Scale Unsupervised Learning. In *International Conference on Machine Learning*, June 2012.
- [35] Y. Lecun, L. Bottou, Y. Bengio, and P. Haffner. Gradient-based learning applied to document recognition. *Proceedings of the IEEE*, 86, 1998.
- [36] N. Maeda, S. Komatsu, M. Morimoto, and Y. Shimazaki. A  $0.41\mu\text{A}$  standby leakage 32kb embedded sram with low-voltage resume-standby utilizing all digital current comparator in 28nm hkgm cmos. In *International Symposium on VLSI Circuits (VLSIC)*, 2012.
- [37] A. Majumdar, S. Cadambi, M. Becchi, S. T. Chakradhar, and H. P. Graf. A Massively Parallel, Energy Efficient Programmable Accelerator for Learning and Classification. *ACM Transactions on Architecture and Code Optimization*, 9(1):1–30, Mar. 2012.
- [38] R. E. Matick and S. E. Schuster. Logic-based eDRAM: Origins and rationale for use. *IBM Journal of Research and Development*, 49(1):145–165, Jan. 2005.
- [39] P. Merolla, J. Arthur, F. Akopyan, N. Imam, R. Manohar, and D. Modha. A digital neurosynaptic core using embedded crossbar memory with 45pJ per spike in 45nm. In *IEEE Custom Integrated Circuits Conference*, pages 1–4. IEEE, Sept. 2011.
- [40] Micron. Ddr3 sdram rdimm datasheet, [http://www.micron.com/~med/ia/documents/products/data%20sheet/modules/parity\\_rdimm/jsf18c1\\_gx72pdz.pdf](http://www.micron.com/~med/ia/documents/products/data%20sheet/modules/parity_rdimm/jsf18c1_gx72pdz.pdf).
- [41] V. Mnih and G. Hinton. Learning to Label Aerial Images from Noisy Data. In *Proceedings of the 29th International Conference on Machine Learning (ICML-12)*, pages 567–574, 2012.
- [42] M. Muller. Dark Silicon and the Internet. In *EE Times "Designing with ARM" virtual conference*, 2010.
- [43] NVIDIA. Tesla K20X GPU Accelerator Board Specification. Technical Report November, 2012.
- [44] W. Qadeer, R. Hameed, O. Shacham, P. Venkatesan, C. Kozyrakis, and M. A. Horowitz. Convolution engine: balancing efficiency & flexibility in specialized computing. In *International Symposium on Computer Architecture*, 2013.
- [45] R. Salakhutdinov and G. Hinton. An Efficient Learning Procedure for Deep Boltzmann Machines. *Neural Computation*, 2006:1967–2006, 2012.
- [46] J. Schemmel, J. Fieres, and K. Meier. Wafer-scale integration of analog neural networks. In *International Joint Conference on Neural Networks*, pages 431–438. Ieee, June 2008.
- [47] O. Temam. A Defect-Tolerant Accelerator for Emerging High-Performance Applications. In *International Symposium on Computer Architecture*, Portland, Oregon, 2012.
- [48] V. Vanhoucke, A. Senior, and M. Z. Mao. Improving the speed of neural networks on CPUs. In *Deep Learning and Unsupervised Feature Learning Workshop, NIPS 2011*, 2011.
- [49] G. Venkatesh, J. Sampson, N. Goulding-hotta, S. K. Venkata, M. B. Taylor, and S. Swanson. QsCORES : Trading Dark Silicon for Scalable Energy Efficiency with Quasi-Specific Cores Categories and Subject Descriptors. In *International Symposium on Microarchitecture*, 2011.
- [50] G. Wang, D. Anand, N. Butt, A. Cestero, M. Chudzik, J. Ervin, S. Fang, G. Freeman, H. Ho, B. Khan, B. Kim, W. Kong, R. Krishnan, S. Krishnan, O. Kwon, J. Liu, K. McStay, E. Nelson, K. Nummy, P. Parries, J. Sim, R. Takalkar, A. Tessier, R. Todi, R. Malik, S. Stiffler, and S. Iyer. Scaling deep trench based edram on soi to 32nm and beyond. In *IEEE International Electron Devices Meeting (IEDM)*, 2009.